Received: 23 June 2022 | Revised: 8 September 2023 | Accepted: 12 September 2023

DOI: 10.33012/navi.624

ORIGINAL ARTICLE

Effect of User Antenna Group Delay Variation Error on Advanced RAIM

Eugene Bang | Mihaela-Simona Circiu | Stefano Caizzone | Markus Rippl | Omar Garcia Crespillo

German Aerospace Center (DLR), Germany

Correspondence
O. Garcia Crespillo
Institute of Communication and Navigation, German Aerospace Center (DLR), Muenchenerstr 20, 82234, Wessling, Germany.
Email: Omar.GarciaCrespillo@dlr.de

Abstract

This study investigates the impact of antenna group delay variation (AGDV)-induced error on advanced receiver autonomous integrity monitoring. We model the AGDV error contribution not only as a measurement bias but also as a random process sigma term in protection-level computations by using AGDV errors analyzed within the European Dual Frequency Multipath Model for Aviation (DUFMAN) project. We also apply the new multipath and AGDV error models developed for aviation use to assess the availability of localizer performance with vertical guidance down to 200 feet. The results show that the fraction of users with ≥99.5% availability increases by approximately 5% when the newly derived DUFMAN models are used. In contrast, considering the AGDV effect alone as the worst-case bias has a weaker impact at the current user range accuracy standard.

Keywords

ARAIM, aviation (and availability), integrity monitoring, multipath

1 | INTRODUCTION

Global navigation satellite system (GNSS) radio signals on different carrier frequencies experience time delay, referred to as a (differential) group delay, while passing through different analog and digital signal paths, including the satellite transmitting antenna and the receiving antenna (Caizzone, Circiu, Elmarissi, Enneking, & Felux, 2019; Kaplan & Hegarty, 2017). Such timing delay can result in pseudorange measurement biases within the user receiver. The effect of the group delay caused by the satellite antenna can be mitigated by using satellite broadcast parameters such as the timing group delay (T_{GD}) and group delay differential corrections for different frequencies (IS-GPS-200N, 2022; OS SIS ICD, 2021).

At the receiver side, the receiver antenna group delay would have no impact on user position accuracy if the user antenna pattern were isotropic and hence the group delay were constant over a range of angles, because the group-delay-induced errors would be projected into the receiver clock bias estimation. However, in the literature, it has been shown that antenna group delay variation (AGDV) with respect to frequency and angle of arrival due to nonuniformity in the user antenna

pattern results in pseudorange measurement biases (Caizzone, Circiu, Elmarissi, Enneking, & Felux, 2019; Wanninger et al., 2017).

Since the initial publication of the standard multipath model for the global positioning system (GPS) L1 signal for aviation purposes (Murphy et al., 1996, 2000), the effect of pseudorange group delay variation versus direction of arrival due to antenna effects has been identified as a partially overlooked error source, as there is no allocation for this term in the protection-level (PL) equation (Working Group C. ARAIM Technical Subgroup, 2016). Because this error source was not removed from the data used to validate the standard multipath model, the group delay variation for the antennas tested has been partially included in the multipath model. Furthermore, using an antenna other than that used for multipath model validation could result in larger group delay variation, which would result in error contributions not included in the multipath model.

Slowly varying bias-like errors present in measurements can stem from a number of sources, including clock and orbit biases, nominal signal deformation biases, inter-frequency biases, and satellite antenna biases. These sources were identified and evaluated for the GPS constellation by Walter et al. (2018), with each error contributing to a total expected value of 75 cm. In particular, the contribution of GPS satellite antenna phase and group delay variations to the bound accounts for approximately 40 cm (Haines et al., 2012; Walter et al., 2018). The expected value of 75 cm has been consistently used in numerous works on advanced receiver autonomous integrity monitoring (ARAIM) as a suitable maximum bias term, b_{nom}, to bound these errors under nominal conditions. The constant bound, provided to the receiver via the integrity support message (ISM), is considered in the current baseline user algorithm for ARAIM (Blanch et al., 2015) and has been introduced in the document (Working Group C. ARAIM Technical Subgroup, 2016) recently updated from the WG-C Advanced RAIM Technical Subgroup. However, unlike the satellite antenna bias contribution in b_{nom}, the impact of user AGDV on user position is currently considered to be integrated into the receiver code noise and multipath (CNMP) term within the legacy error model (Working Group C. ARAIM Technical Subgroup, 2016), which may lead to an underestimation of user PLs. Therefore, during ARAIM development, it is crucial to predict and review the performance for modeling error sources in the worst case.

In previous work (M. Circiu et al., 2020), we developed airborne multipath models for the Dual Frequency Multipath Model for Aviation (DUFMAN) project by collecting GPS and Galileo measurements from several test flights using aviation GNSS antenna and receivers. The multipath error models were derived by characterizing the user antenna error biases and separating their contribution from observed multipath errors. Griggs et al. (2020) addressed the impact of the preliminary DUFMAN multipath and user antenna error models on ARAIM performance. Particularly, in that investigation, the antenna-induced error contribution was considered in the nominal bias term (i.e., b_{nom}) of the current ARAIM user algorithm; however, accounting for the antenna effect within the bias term may not be completely optimal (Griggs et al., 2020). More recently, the antenna errors were accounted for with a sigma term, which is added to multipath-only models (Circiu et al., 2021). Although the models were based on extensive dual-frequency dual-constellation data collection and precise estimation processes of multipath and antenna errors, they were derived in terms of the root mean square (RMS) of the corresponding error distributions in order to maintain compliance with the existing GPS L1 model. Thus, if the new models appear to be overly optimistic for ARAIM implementation, more rigorous methods for integrity purposes may be needed.

This paper extends upon the existing approach (Griggs et al., 2020) to examine the impact of pseudorange error caused by user AGDV, denoted as AGDV (induced) error, on ARAIM. We also present different approaches to account for antenna errors in ARAIM. For this purpose, user-satellite geometries are first

simulated based on 24 GPS/Galileo constellations and a predefined global user grid formation for ten sidereal days, which corresponds to the repetition period of the Galileo constellation (Working Group C. ARAIM Technical Subgroup, 2016). Next, user AGDV errors in signals propagated to the users are computed based on actual antenna measurements, as presented in our previous investigation (M. Circiu et al., 2020; Circiu et al., 2019). In this study, we apply two approaches to assess the effect of AGDV-induced errors and the new multipath model on ARAIM performance: measurement and position domain analysis.

We first analyze the position error due to antenna errors based on instantaneous user geometry and the corresponding set of AGDV errors. In this study, we investigate user antenna errors for different constellations and frequencies, such as the GPS L1/L5 and Galileo E1/E5a frequencies and a GPS/Galileo dual-frequency ionosphere-free (IF) combination. Based on empirical observations for the different cases, the statistical properties of the antenna error projected to the position domain are analyzed. Relevant overbounding distributions are also constructed by applying the Gaussian cumulative distribution function (CDF) overbounding method (DeCleene, 2000). We then apply the resulting Gaussian parameters for the overbounding distributions to the current user PL computation. In addition to the bias effect, the newly developed dual-frequency multi-constellation multipath model is also substituted for the multipath contribution within the ARAIM airborne error model.

Next, a Gaussian overbounding model of the antenna errors is derived in the measurement domain as a function of satellite elevation angle. For this, the antenna-induced errors for the IF combination of GPS L1/L5 and Galileo E1/E5a are computed using the same user–satellite geometries examined for the position domain analysis. The AGDV-induced errors are then sorted into elevation bins of 5° separation. The mean and standard deviation of the bias errors in each bin are computed and used to normalize the bias errors. Based on the distribution of normalized antenna errors, Gaussian overbounds are determined for different elevation bins. In this case, we apply the sum of squares of the upper bound on the AGDV errors and the DUFMAN multipath model for the airborne error model.

To examine the impact of the newly proposed AGDV error models on ARAIM performance, we conduct ARAIM service volume simulations for localizer performance with vertical guidance down to 200 feet (LPV-200). All simulations are carried out using the Stanford MATLAB Algorithm Availability Simulation Tool (MAAST) (*MATLAB Algorithm Availability Simulation Tool*, 2021) for ARAIM with some modifications and the key simulation parameters outlined by the Working Group C, ARAIM Technical Subgroup (2016). Several simulation scenarios are investigated in our approach:

1. Baseline case: Current CNMP model (Blanch et al., 2015)
2. New DUFMAN multipath and antenna error models (root sum squared together) instead of the legacy CNMP
3. DUFMAN multipath model implemented in the CNMP term and the overbounding model for antenna-induced position errors in the PL computation
4. Root sum of squares of the DUFMAN multipath model and the overbounding antenna pseudorange error
5. DUFMAN multipath model in the CNMP term and the AGDV error considered within a bias term added to PLs

This work examines the increase in PL that can be expected in the scope of ARAIM by thoroughly considering the AGDV effect. This paper is organized as follows. In Sections 2, the new DUFMAN error model is briefly introduced, and the methodology for AGDV error modeling is presented in Sections 3 and 4. Simulation results are then discussed in Section 5, and Section 6 concludes with remarks for future work.

2 | DUFMAN MULTIPATH AND AGDV-INDUCED ERROR MODELS

The current baseline ARAIM airborne algorithm (Blanch et al., 2015) employs the Airborne Accuracy Designator – Model A (AAD-A) (Murphy et al., 2000) with a GPS L1/L5 CNMP budget that consists of the airborne multipath (σ_{MP}) contribution and receiver tracking noise (σ_{noise}) contribution:

$$\sigma_{CNMP} = \sqrt{\frac{f_{L1}^4 + f_{L5}^4}{\left(f_{L1}^2 - f_{L5}^2\right)^2}} \sqrt{\sigma_{MP}^2 + \sigma_{Noise}^2} \tag{1}$$

where $f_{L1\ (or\ L5)}$ indicates the frequency (L1 = 1575.42 MHz or L5 = 1176 MHz) and the same level of multipath and noise is assumed for both frequencies. As mentioned in Section 1, the σ_{MP} term in the legacy airborne error model contains the antenna error contribution due to AGDV. However, the multipath estimation process includes removal of the carrier-phase cycle ambiguity, which is achieved by leveling the processed data, and some of the slowly varying (i.e., bias-like) AGDV-induced error would have been eliminated during this step.

Therefore, in the derivation of the DUFMAN models, the AGDV error contribution (i.e., σ_{AGDV}) was separated from the multipath error contribution for single-frequency L1/E1 and L5/E5a and a dual-frequency IF combination to rigorously characterize the errors. Final airborne user error models for different frequencies have been proposed for those frequency combinations by combining the two error contributions (Circiu et al., 2021) as follows:

$$\sigma_{MP\ \&\ AGDV} = \sqrt{\sigma_{MP}^2 + \sigma_{AGDV}^2} \tag{2}$$

Moreover, in the DUFMAN models, the terms σ_{MP} and σ_{AGDV} were derived such that the resulting standard deviation (or RMS) of multipath estimates (or AGDV estimates) is bounded by the sigma term, σ_{MP} (or σ_{AGDV}), i.e., not in the form of an overbounding sigma for integrity purposes, in order to be consistent with the legacy architecture of the error budget and the error bounding concepts for GPS L1 (Circiu et al., 2021). Thus, in this work, we apply a few approaches to model the AGDV error contribution as an overbounding sigma in the worst-case scenario, as described in the following sections.

Figure 1 shows the presented multipath and AGDV error RMS model ($\sigma_{MP\&AGDV}$) for the IF combination (blue), which will be used for the ARAIM performance simulations in this work. Because the single-frequency model is not addressed in this study, it is not presented in this figure. The red curve indicates the conventional GPS L1 multipath error bound (Murphy et al., 2000), which is multiplied by a factor of 2.59 for the dual-frequency IF combination. As reported by Circiu et al. (2021), the proposed DUFMAN model is significantly less conservative than the legacy GPS L1 model for low elevation angles, for instance, at angles smaller than approximately 40°. Note that the derivation of the legacy model was based on conservative assumptions on receiver thermal noise and interference and the antenna error (Murphy et al., 2000), and old equipment were considered for the development of the model. Although the new DUFMAN model was developed via the same methodology, the new model considered less-conservative assumptions on the antenna error (M.-S. Circiu et al., 2020).

Figure 2 (left) shows the new σ_{MP} bound (i.e., not including the AGDV contribution) for the IF combination. Because the performances of the multipath

models derived for Galileo and GPS were comparable, a common model has been proposed for the IF combination (Circiu et al., 2021). The new model is shown to be significantly less conservative than the legacy GPS model for low elevations.

Figure 2 (right) shows the DUFMAN σ_{AGDV} bound obtained by isolating the AGDV contribution from the multipath estimation process. Because the performances of L1/E1 and L5/E5a were comparable (Circiu et al., 2021), a single shared model has been presented, as described for the multipath model. The results demonstrate that the significant elevation dependency of the combined model shown above comes arises from the σ_{AGDV} model. Although AGDV errors are deterministic for one antenna, it is considered too complicated to apply a different calibration step for every antenna in practice. Thus, it is preferable to model the error with a single parameter, such as the standard deviation (see Figure 2 [right]) from a zero-mean Gaussian distribution, in a manner similar to methods employed for other error sources.

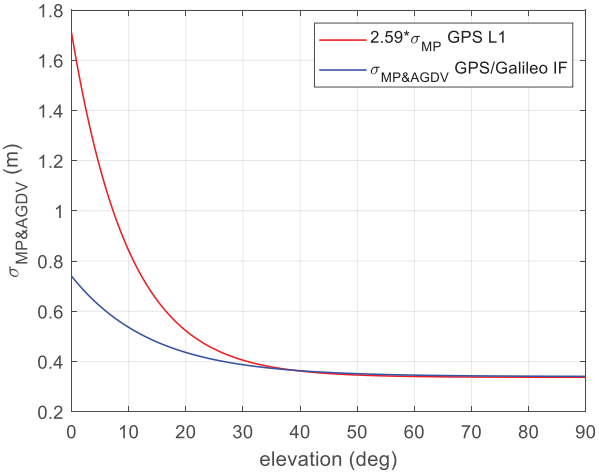

FIGURE 1 The recently proposed DUFMAN multipath and AGDV error models for the dual-frequency IF combination are shown in blue (Circiu et al., 2021). The red curve shows the conventional GPS L1 multipath sigma bound, which is increased to 2.59 times that of the original L1 multipath model (Murphy et al., 2000) for the IF combination.

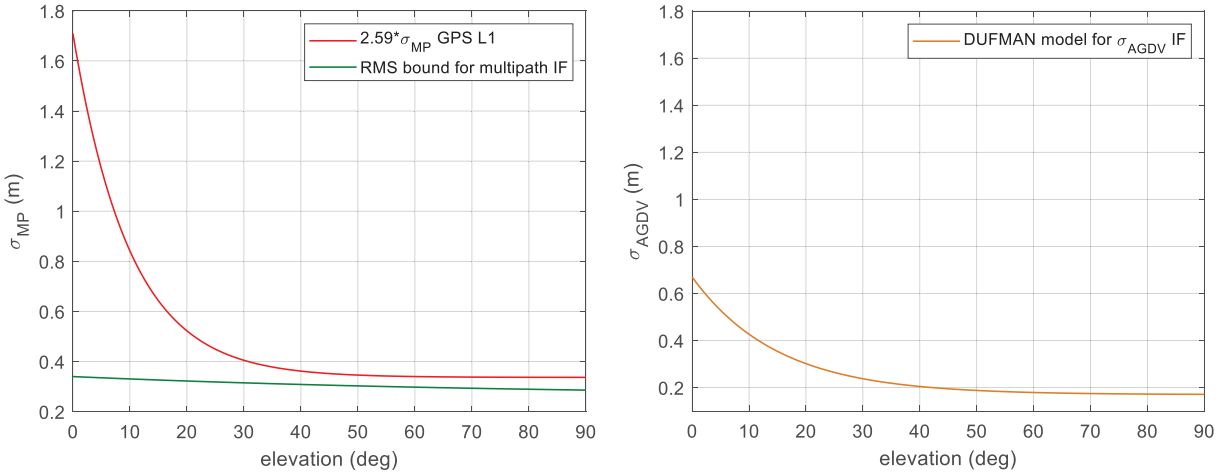

FIGURE 2 New DUFMAN multipath error bound for the dual-frequency IF combination (left) and AGDV error bound for the IF combination for GPS and Galileo (right)

TABLE 1
Proposed Models for Multipath and AGDV Errors

Type	Model E1	Model E5a	Model IF
Multipath only (σ_{MP})	$0.11 + 0.03 * e^{-\theta/80}$	$0.07 + 0.06 * e^{-\theta/50}$	$0.26 + 0.08 * e^{-\theta/80}$
AGDV only (σ_{AGDV})	$0.065 + 0.2 * e^{-\theta/14}$	$0.065 + 0.2 * e^{-\theta/14}$	$0.17 + 0.5 * e^{-\theta/15}$
Multipath & AGDV ($\sigma_{MP\&AGDV}$)	$0.13 + 0.17 * e^{-\theta/13}$	$0.11 + 0.18 * e^{-\theta/15}$	$0.34 + 0.4 * e^{-\theta/14}$

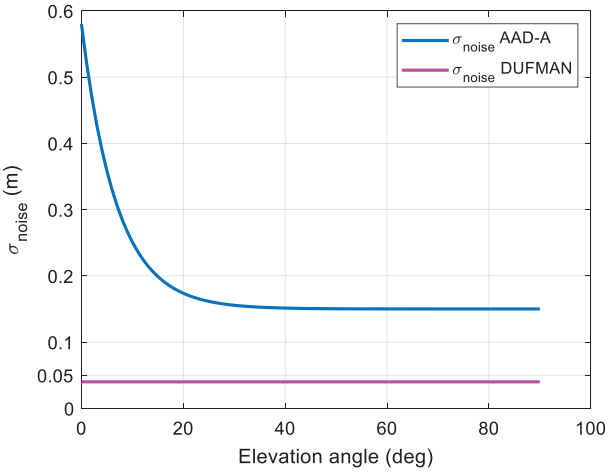

FIGURE 3 Existing receiver noise and interference error model used for the current ARAIM algorithm (blue) and the constant DUFMAN model value of 0.04 m (magenta)

Table 1 summarizes the DUFMAN models derived for the multipath-only model, AGDV-only models, combined models for L1/E1 and L5/E5a, and dual-frequency IF combination. Note that the DUFMAN models provide Gaussian models with zero mean and the standard deviations summarized in Table 1. More details of the newly proposed models, including the methodologies used, can be found in the report by Circiu et al. (2021).

Lastly, the combined sigma model in Equation (2) should be augmented by the code noise error component such that the combined user model complies with the legacy CNMP model as follows:

$$\sigma_{CNMP} = \sqrt{\sigma_{MP}^2 + \sigma_{AGDV}^2 + \sigma_{noise}^2} \tag{3}$$

In the DUFMAN studies, the final multipath models were derived with the assumption that σ_{noise} is 0.03 m for all signals and 0.04 m for the IF combination (M. Circiu et al., 2020). A more detailed examination of the receiver noise was performed in a recent study (Harris et al., 2020), and the obtained values were slightly lower than the values assumed in DUFMAN. However, the impact of the different models is considered marginal, and in this paper, the value of 0.04 m assumed in DUFMAN is used for simulation purposes.

Figure 3 shows the AAD-A results (Murphy et al., 2000) used to bound the receiver thermal noise and interference error for the ARAIM framework (blue curve), represented as a function of elevation angle according to the recommendation of airborne receiver minimum operational performance standards (MOPS) (RTCA SC-159, 2004, 2016). The magenta line shows the constant model value of 0.04 m, which is more optimistic than the legacy model for the noise bound. However, it should be noted that the DUFMAN values were conservatively estimated through initial studies and require further confirmation.

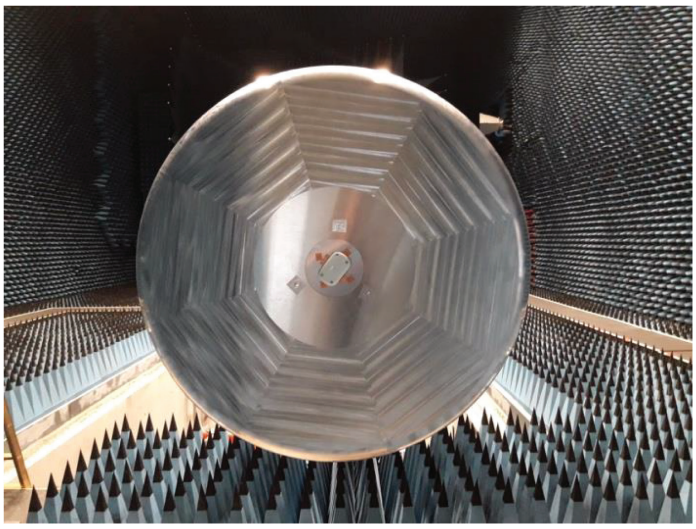

FIGURE 4 Commercially available avionic antenna as measured (on a ground plane with rolled edges, as specified in the antenna MOPS (RTCA, 2006)) at the DLR anechoic chamber

3 | AGDV ERROR ESTIMATES

The antenna-induced errors for the pseudorange were estimated from measurements obtained in an anechoic antenna measurement chamber over all GNSS bands. The measured antenna transfer function was then processed through an ideal receiver, and the residual error was obtained, as shown in our prior work (Caizzone, Circiu, Elmarissi, Enneking, & Felux, 2019). Because the receiver components are ideal, the pseudorange error obtained from this technique results only from antenna imperfections (i.e., AGDV behavior); thus, we refer to the pseudorange range as AGDV (pseudorange) error hereafter. Note that the interaction of the antenna with the installation platform influences the results. As suggested in antenna MOPS (RTCA, 2006), the antenna was measured on a rolled-edge ground plane (Figure 4) to model, at best, the metallic vicinity of the antenna for inclusion in the antenna-intrinsic error. The interactions from further elements of the aircraft were modeled through multipath effects/errors, as presented in Equation (3) and as also foreseen in EUROCAE (2019).

Multiple commercial antennas were examined at the German Aerospace Center (DLR), and indeed, each antenna showed specific errors, different from those of other antennas. For the derivation of the initial AGDV models, an antenna, fitting into the standard ARINC 743 footprint and having group delay variations for L1/E1 and L5/E5a frequencies close to the allowable limits, was chosen to be representative of a minimally MOPS-compliant commercial antenna (RTCA SC-159, 2018) and was also used in this work. The AGDV characterization results are presented in Section 2.4.

4 | METHODS

This section presents a few methods for evaluating the impact of AGDV error on ARAIM. The new DUFMAN multipath and AGDV error models will first be described, and three different approaches for modeling the user antenna bias error will then be explained. The details of each step are described in the following sections.

4.1 | Considering User Antenna Errors Caused by AGDV in the Position Domain

As mentioned previously, there is no allocation for the antenna bias caused by group delay variations in the standard PL equation for ARAIM. Moreover, the manner in which the antenna-induced error should be included within the standard ARAIM user algorithm, for instance, as a deterministic bias term or as a random process, has yet to be standardized (Working Group C. ARAIM Technical Subgroup, 2016). Thus, this paper aims to evaluate how the AGDV-induced error affects ARAIM performance by investigating different methods for considering its impact and incorporating it into the PL. In this section, we first describe the modeling of position errors caused by AGDV and then directly incorporate the resulting models into the current PL equation. In subsequent sections, we present other approaches in which AGDV-associated errors are modeled in the range domain using the sigma and bias terms. Lastly, the impact of the different models on ARAIM performance are examined.

The AGDV errors for L1/L5 and E1/E5a dual-frequency measurements are estimated by using the following IF combination of single-frequency AGDV errors estimated on the different frequencies, L1/ L5 (or E1/E5):

$$b_{AGDV_{IF}} = \frac{f_{L1}^2}{f_{L1}^2 - f_{L5}^2} b_{AGDV_{L1}} - \frac{f_{L5}^2}{f_{L1}^2 - f_{L5}^2} b_{AGDV_{L5}} \tag{4}$$

in which $b_{AGDV_{L1}}$ and $b_{AGDV_{L5}}$ are AGDV errors estimated for the L1 and L5 frequencies, respectively. This work uses the AGDV error estimates collected and analyzed in the DUFMAN project (Circiu et al., 2021) to derive the σ_{AGDV} bound shown in Figure 2 for characterizing position errors caused by AGDV errors. We then derive the errors that contribute to the position solution by eliminating the common bias over satellites in view that will affect the receiver clock bias estimation in order to characterize position errors caused by the antenna contribution. For this, antenna residual errors to be projected into the position domain are calculated as in Equation (5). Ie we consider GPS and Galileo constellations for ARAIM, the bias removal is performed independently for each constellation:

$$\delta b^j_{AGDV_{IF},i} = b^j_{AGDV_{IF},i} - \frac{1}{N_j} \sum_i^{N_j} b^j_{AGDV_{IF},i} \tag{5}$$

where i is the satellite index, j is the constellation index, N_j is the number of satellites in view within constellation j ($j = 1, 2$, i.e., GPS or Galileo), and $\delta b^j_{AGDV_{IF},i}$ is the antenna bias residual for the measurement from the i-th satellite within constellation j.

The AGDV residual error for each satellite at each epoch is then projected into the position domain as follows:

$$\boldsymbol{e} = \begin{bmatrix} e_1 \\ \vdots \\ e_5 \end{bmatrix} = \boldsymbol{S} \begin{bmatrix} \delta b^1_{AGDV_{IF},1} \\ \vdots \\ \delta b^1_{AGDV_{IF},N_1} \\ \delta b^2_{AGDV_{IF},1} \\ \vdots \\ \delta b^2_{AGDV_{IF},N_2} \end{bmatrix} \qquad \text{where } \boldsymbol{S} = (\boldsymbol{G}^T \boldsymbol{W} \boldsymbol{G})^{-1} \boldsymbol{G}^T \boldsymbol{W} \tag{6}$$

Here, $\boldsymbol{e}$ is an vector whose components are antenna error contributions projected to the states (i.e., position errors and clock biases for GPS and Galileo), $\boldsymbol{G}$ is a geometry matrix, and $\boldsymbol{W}$ is a weight matrix determined from pseudorange measurement error models such as satellite ephemeris/clock, tropospheric delay, and CNMP error models.

More specifically, we have the following:

$$\mathbf{W} = \Sigma^{-1} \tag{7}$$

where:

$$\Sigma = \begin{pmatrix} \sigma_1^2 & \cdots & 0 \\ \vdots & \ddots & \vdots \\ 0 & \cdots & \sigma_{N_1+N_2}^2 \end{pmatrix} \tag{8}$$

For dual-frequency-based ARAIM, variances for each measurement, σ_i^2, are constructed by considering the satellite ephemeris and clock error, tropospheric error, and CNMP error components (Blanch et al., 2015):

$$\sigma_i^2 = \sigma_{URA,i}^2 + \sigma_{tropo,i}^2 + \sigma_{user,i}^2 \tag{9}$$

where i is the satellite index, $\sigma_{URA,i}$ is the standard deviation of the clock and ephemeris error for the i-th satellite used for integrity purposes, $\sigma_{tropo,i}$ is the standard deviation of the tropospheric delay corresponding to the signal from the i-th satellite, and $\sigma_{user,i}$ is the standard deviation of the airborne multipath and interference error (equivalent to the user CNMP error in this paper) relevant to the signal from the i-th satellite.

The AGDV effect should be considered in addition to the existing error components in Equation (9), represented as $\boldsymbol{\varepsilon}_{\boldsymbol{others}}$, to construct the projection from the measurement domain to the position domain as follows:

$$\Delta x_v = \hat{x}_v - x_v = \boldsymbol{S}_v \boldsymbol{\varepsilon} = \boldsymbol{S}_v (\boldsymbol{\varepsilon}_{\boldsymbol{others}} + \boldsymbol{\delta b}_{\boldsymbol{AGDV}}) = \boldsymbol{S}_v \boldsymbol{\varepsilon}_{\boldsymbol{others}} + \boldsymbol{S}_v \boldsymbol{\delta b}_{\boldsymbol{AGDV}} \tag{10}$$

where v is the index for the state, e.g., the east, north, and up components. $\boldsymbol{S}_v$ is a row vector of the projection matrix for each v-th state, and Δx_v is the state estimation error, e.g., the position error in the up coordinate. $\hat{x}_v$ and x_v are the state estimate and the true value of the state, respectively. $\boldsymbol{\varepsilon}$ is the measurement error vector, $\boldsymbol{\varepsilon}_{\boldsymbol{others}}$ is the measurement error due to satellite ephemeris/clock error, tropospheric error, and multipath, and $\boldsymbol{\delta b}_{\boldsymbol{AGDV}}$ is the antenna bias error vector.

Equation (10) implies that the two random variables (i.e., the AGDV contribution and the other contribution to the position error) can be combined into a single random variable by the root sum square of their variances, which will be applied to incorporate the AGDV effect into the PL calculation in this section.

In the remainder of the paper, for simplicity, we assume the state of interest as the vertical position coordinate. In Equation (10), the error vector, $\boldsymbol{\varepsilon}_{\boldsymbol{others}}$, contains pseudorange errors for different satellites due to the error sources represented in Equation (9). As shown in Equation (10), the projection by matrix $\boldsymbol{S}$ is a linear transformation. Therefore, if the antenna error, represented as $\boldsymbol{\delta b}_{\boldsymbol{AGDV}}$, is statistically independent of $\boldsymbol{\varepsilon}_{\boldsymbol{others}}$ in the range domain, these two terms are also independent in the position domain. ARAIM provides the vertical PL (VPL), the region assured to contain the indicated vertical position with the required probability for a specific navigation mode, such that the user can assess the integrity risk at a given

measurement epoch. The VPL equation for ARAIM (Blanch et al., 2015) is shown in Equation (11):

$$2Q\left(\frac{VPL-b_0}{\sigma_0}\right)+\sum_{k=1}^{N}\left(P_{fault,k}\cdot Q\left(\frac{VPL-T_k-b_k}{\sigma_k}\right)\right)=PHMI_{monitored} \tag{11}$$

where Q is the tail probability of a zero-mean unit Gaussian distribution, σ_0 is the standard deviation of the all-in-view position solution (H_0), σ_k is the standard deviation of fault-tolerant position solution for H_k ($k = 1, \ldots, N$), b_k is the nominal bias for H_k ($k = 0, 1, \ldots, N$), $P_{fault,\,k}$ is the prior probability of fault for H_k ($k = 1, \ldots, N$), T_k is the threshold for the solution separation (SS) test for the k-th fault mode, and $PHMI_{monitored}$ is the integrity risk allocation for monitored faults (in this example, for the vertical coordinate).

If the position error caused by the AGDV effect in the measurement domain has a Gaussian distribution for the k-th fault mode, i.e., $N(b_{k,\,AGDV}, \sigma_{k,\,AGDV})$, the standard deviation and mean can be directly incorporated in the PL equation, as shown in Equation (12). Note that, in this section, the Gaussian overbound published in the standards is applied to model the AGDV-induced position error while ensuring a margin of conservatism for integrity purposes. Because the AGDV effect can be considered as statistically independent from the other error contribution, the worst-case impact of the bias due to the AGDV error ($b_{k,\,AGDV}$) is considered by augmenting the nominal bias term b_k:

$$2Q\left(\frac{VPL-b_0-b_{0,\,AGDV}}{\sqrt{\sigma_0^2+\sigma_{0,\,AGDV}^2}}\right)+\sum_{k=1}^{N}P_{fault,k}Q\left(\frac{VPL-T_k-b_k-b_{k,\,AGDV}}{\sqrt{\sigma_k^2+\sigma_{k,\,AGDV}^2}}\right) \tag{12}$$
$$=PHMI_{monitored}$$

To characterize the distribution of the antenna-induced error such that the PL (the term VPL) is determined from Equation (12), we first examine the antenna error contribution projected to the position error, as shown in Equation (10), by running a vertical ARAIM (V-ARAIM) service volume simulation with the ISM parameters and critical parameters listed in Table 2. All of the simulations performed in this work are based on a set of ISM parameters defined for the current baseline airborne ARAIM algorithm outlined by the Working Group C, ARAIM Technical Subgroup (2016). Particularly, the value of $P_{const} = 10^{-8}$ for the GPS constellation-wide fault is consistent with the GPS constellation specification outlined in the fifth edition (the latest edition) of the GPS Standard Positioning Service Performance Standard. Thus, the value of 10^{-8} is chosen in our analysis; however, there have been discussions on other possible values because of the uncertainty regarding whether the amount of data corresponding to observed operational data during GPS history is sufficient to thoroughly verify such a low probability. Thus, future work should include further validation and updates if necessary.

For the simulation, we used the MAAST for ARAIM (*MATLAB Algorithm Availability Simulation Tool*, 2021) with some modifications. All of the simulations in this work were performed for a period of ten sidereal days, which corresponds to the repetition period of the Galileo constellation, with an interval of 600 s over a user grid formation of 5° by 5°. Because the position error distribution should be different for different fault types, we investigated the fraction of different fault modes separately. For the parameters and 24 GPS and 24 Galileo constellations assumed by the Working Group C, ARAIM Technical Subgroup (2016), three different types of fault modes were primarily observed in our investigation: a fault-free mode,

TABLE 2
ARAIM Simulation Parameters

Parameter	Description
Constellation	24 GPS + 24 GAL
b_{nom}	0.75 m
σ_{URE}	GPS (Walter & Blanch, 2015) / GAL (Perea et al., 2017)
σ_{URA}	1 m for GPS/GAL (2.5 m for H-ARAIM)
P_{sat}	10^{-5}
P_{const}	GPS: 10^{-8} / GAL: 10^{-4}
Mask angle	5°
User grid formation	5° by 5°
Simulation time interval	10 min
Simulation duration	10 days

TABLE 3
Fraction of Different Fault Modes for ARAIM Over 10 Days

All in view	Single-satellite fault	Dual-satellite fault	GAL constellation fault
~5.3%	~89.3%	0%	~5.3%

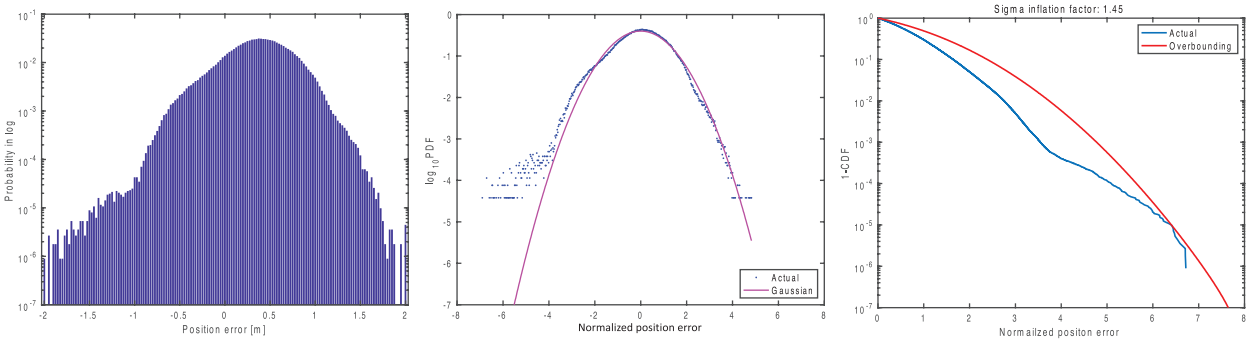

FIGURE 5 Histogram of vertical position errors caused by the AGDV effect obtained under the Galileo constellation fault (left); PDF of the normalized vertical position error based on the Galileo constellation fault ($P_{GAL} = 10^{-5}$) (middle); 1–CDF of the normalized error (blue) and the overbounding curve when an inflation factor of 1.45 is applied (red) (right)

GPS/Galileo single-satellite failure, and Galileo constellation fault, as displayed in Table 3. Table 3 also shows that the GPS and Galileo single-satellite faults are dominant for the V-ARAIM implementation, and the fault-free mode is observed as often as Galileo constellation faults.

Observing that these three fault modes are more dominant than other multiple-satellite fault modes, the error caused by AGDV is characterized by the Gaussian parameters, i.e., $b_{k,\,AGDV}$, $\sigma_{K,\,AGDV}$, with a focus on the three fault hypotheses in this work. Figure 5 shows a histogram of position errors caused by the AGDV residual errors in Equation (6) in the vertical position coordinate for the Galileo constellation fault (left), the probability density of the position error normalized by its mean and standard deviation (middle), and 1 – CDF of the normalized position errors (right). Note that as mentioned above, the position error resulting from the antenna contribution is our main interest in this examination.

The histogram shows that the distribution has a mean of approximately 0.3 m, and the maximum position error due to the antenna error in the vertical coordinate is approximately 1.7 m for the Galileo constellation fault when the antenna-induced pseudorange error is considered.

TABLE 4
Position Error Statistics for the Fault-Free Case, Single-Satellite Fault Mode, and Galileo Constellation Fault Mode

Fault mode	Vertical		Horizontal (east)		Horizontal (north)	
	$b_{k,AGDV}$ [m]	$\sigma_{k,AGDV}$ [m]	$b_{k,AGDV}$ [m]	$\sigma_{k,AGDV}$ [m]	$b_{k,AGDV}$ [m]	$\sigma_{k,AGDV}$ [m]
Fault-free (H_0)	0.34	0.25	0.05	0.10	0.16	0.11
Single-sat. fault	0.33	0.26	0.05	0.10	0.12	0.144
GAL cons. fault	0.37	0.51	0.05	0.12	0.16	0.197

In Figure 5 (middle), the errors are normalized by the mean and standard deviation, and the blue dotted curve indicates the probability density function (PDF) of normalized position errors on a log scale. The solid magenta curve is the PDF of a unit Gaussian distribution. Comparison of the empirical PDF and the theoretical standard Gaussian PDF shows that the position error due to the AGDV effect has a non-Gaussian tail, particularly for probabilities lower than 10^{-3}. Therefore, we derive an overbounding variance for the empirical error distribution using the commonly used 1–CDF overbounding method (DeCleene, 2000). In Figure 5 (right), the empirical error distribution with the non-Gaussian tail (blue curve) is bounded by the distribution with the variance inflated by a factor of 1.45 (red curve).

Table 4 summarizes the standard deviation and mean of the position error distribution for the three fault hypotheses for the horizontal and vertical coordinates.

In addition to the position error distributions, we must consider the effect of AGDV on the fault detection threshold T in Equation (11). The ARAIM fault detection threshold, T_k, for the k-th fault mode is determined from the standard deviation of the SS, $\sigma_{SS,k}$, as shown in Equation (13):

$$T_k = K_k \sigma_{SS,k}, \qquad \text{for } k = 1, 2, \cdots, h \tag{13}$$

Here, the factor K_k is obtained from the continuity requirement allocated to the k-th fault hypothesis. The SS, denoted as $d\hat{x}_k$ in Equation (14), is defined as the difference between the all-in-view solution, $\hat{x}_0$, and the subset solution, $\hat{x}_k$, which is determined by using all satellites except the faulty satellites under the hypothesis (Blanch et al., 2015):

$$d\hat{x}_k = \hat{x}_k - \hat{x}_0 = (\mathbf{S_i} - \mathbf{S_0})\mathbf{y} = \mathbf{dS_i}\mathbf{y}, \qquad \text{for } i = 1, 2, \cdots, h \tag{14}$$

Here, $\mathbf{dS_i}$ is the matrix used to generate the SS, and $\mathbf{y}$ indicates a vector whose components are pseudorange measurements for satellites in view. Because the matrix $\mathbf{dS_i}$ is defined as the difference $\mathbf{S_i} - \mathbf{S_0}$ and the projection by $\mathbf{dS_i}$ is linear, we can examine the AGDV effect on the SS domain, as the position errors due to the AGDV residual error were characterized in Equations (6) and (10). The AGVD residual errors are projected from the measurement domain to the SS domain as follows:

$$\epsilon_i = \mathbf{dS_i} \begin{bmatrix} \delta b_{AGDV,1} \\ \vdots \\ \delta b_{AGDV,N} \end{bmatrix}, \qquad \text{for } i = 1, 2, \cdots, h \tag{15}$$

Thus, we simulate position errors for different possible fault modes in different coordinates based on the same ARAIM service volume simulation and perform the same process as those for the position error results in Table 4. The corresponding results are summarized in Table 5.

The $\sigma_{SS,k}$ term in Equation (12) is modified through the root sum square of the baseline σ_{SS} and the overbounding parameters, $\sigma_{SS,AGDV}$, shown in Table 5 for

TABLE 5
Overbounding Parameters for AGDV Errors Projected into the SS Domain in Different Coordinates

Fault mode	Vertical $\sigma_{SS,k,AGDV}$ [m]	Horizontal (east) $\sigma_{SS,k,AGDV}$ [m]	Horizontal (north) $\sigma_{SS,k,AGDV}$ [m]
Single satellite	0.088	0.075	0.104
GAL constellation	0.523	0.117	0.146

different fault modes, and the corresponding threshold T_K is then applied to the VPL equation (Equation (11)). Whereas the bias effect projected into the position domain for different fault modes is considered for integrity purposes, as presented in Table 4, the bias effect on the test is not taken into account for the $\sigma_{SS,AGDV}$ term used to compute the SS test threshold because the monitor threshold is determined for continuity purposes, in line with the current ARAIM development framework (Blanch et al., 2015). The possible bias caused by the AGDV effect is addressed within the term $b_{k,AGDV}$ in the PL calculation in Equation (12).

In this section, the antenna errors due to AGDV were considered in the position domain. However, because this approach is subject to a specific set of satellite constellation geometries and error models, including ISM parameters, it can be far from optimal for a rigorous assessment of the impact of antenna errors, particularly for safety-critical applications. Therefore, although the satellite geometries and error models assumed for the current ARAIM framework are employed for position domain modeling, in this paper, we will consider the approach for simulation purposes and compare it with other methods. Further work is needed to generalize the direct modeling of this error in the position domain.

4.2 | Modeling AGDV-Induced Error as a Random Sigma Term in the Range Domain

Having considered the AGDV error effect in the user PL domain, we now describe another approach for considering the error effect, where the AGDV errors are modeled in the range domain as a random variable (i.e., a sigma term). For this purpose, the AGDV errors in Equation (4) are first collected in the range domain based on the ARAIM simulation described in the previous section. We then apply the same approach as the GNSS airborne antenna MOPS (RTCA SC-159, 2018), where AGDV-induced errors and the corresponding acceptable bounds are modeled as a function of elevation angle. Figure 6 (left) shows a two-dimensional histogram of the number of observations as a function of both the AGDV residual error and the elevation angle. The horizontal axis divides the elevation angles into bins, and the vertical axis divides observations of the residuals into bins. The color of each pixel indicates the number of measurements counted.

The AGDV varies more at low elevations, where the antenna gain pattern is not uniform; thus, Figure 6 (left) shows that the histograms at low elevations are widely spread. In contrast, the group delay variations diminish at high elevations because the patterns are more regular. Therefore, in Figure 6 (right), we obtained higher sigma values (red curve) as the elevation decreases. However, because the antenna is mounted on a metallic ground plane, according to published standards (RTCA, 2006; RTCA SC-159, 2018), small biasing effects appear at high elevations, as shown in the blue curve in Figure 6 (right).

In addition, each histogram for each elevation bin in the left figure contains different antenna group delays for different azimuth angles. Therefore, the delay does not necessarily monotonically increase or decrease with elevation angle, as shown

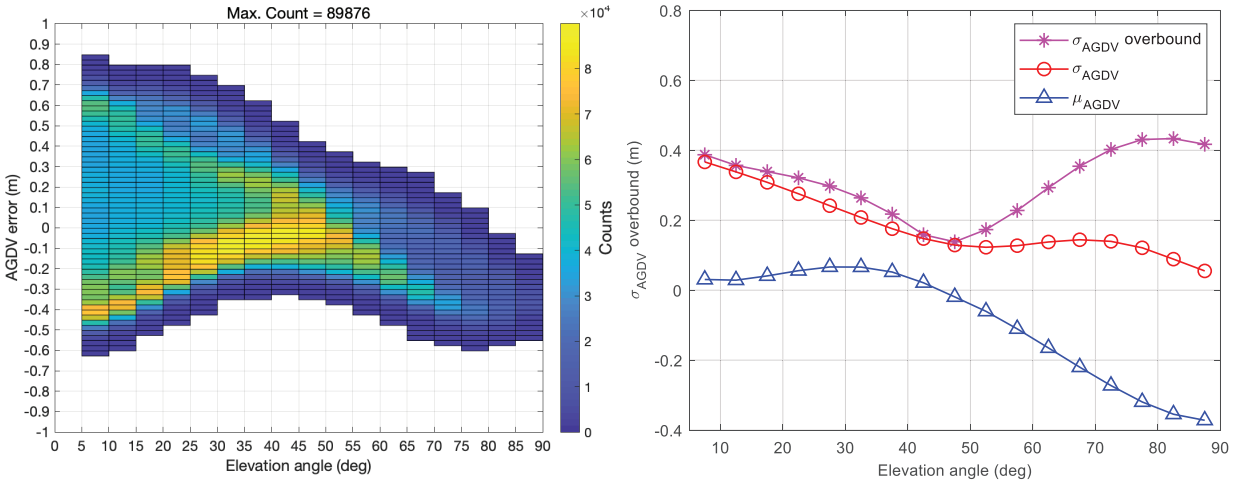

FIGURE 6 The left figure shows histograms of AGDV residual errors for different satellite elevation bins. The right figure shows the empirical means (blue) and standard deviations (red) for different elevation bins and the overbounding sigma terms, $\sigma_{AGDV,\,overbound}$ (magenta).

in Figure 6. In particular, Figure 6 (left) shows that several distributions for different elevation bins have non-zero means and even two different peaks, i.e., the distribution is bimodal. The pair-bounding technique (Rife et al., 2006) was developed to create a pair of overbounding distributions for an actual error distribution that is neither symmetric nor unimodal. However, it has been found to be challenging to meet the pair-bounding condition if the actual error distribution is represented by an empirical histogram (Blanch et al., 2019). A more recent study (Blanch et al., 2019) presented an approach combining the single-CDF (DeCleene, 2000) and the pair-bounding techniques to overcome limitations on the existing pair-bounding technique. This method may be optimal, as it provides a tighter bound than the paired overbounding distribution. However, both methods provide a pair of Gaussian parameters, i.e., a bias and an overbounding sigma, representing the resulting overbounding distribution. In this section, as mentioned above, we consider the error within the random sigma term to be compliant with the current ARAIM error models (Working Group C. ARAIM Technical Subgroup, 2016). In the next section, the AGDV is considered as a bias term in the PL computation in the worst-case scenario.

Here, we take a simple and practical tail bounding approach, where the single CDF bound is applied only to the tails, not the core part, of the actual distribution because the tails lead to the most significant sigma values. In addition, to conservatively account for the non-zero mean, the absolute value of the mean is then added to the overbounding sigma such that the resulting zero-mean Gaussian distribution with the overbounding sigma can overbound the tail of the actual distribution. This simple approach for integrity purposes has often been used to characterize different GNSS errors whose empirical distributions are not symmetric or unimodal, for instance, regarding satellite ephemeris and clock errors (Walter et al., 2018) and ionospheric delay errors in the ground-based augmentation system framework (Lee et al., 2007).

Next, the sigma overbounding method is used to characterize the AGDV residual errors as follows. The mean (μ_{AGDV}) and standard deviation (σ_{AGDV} of the residuals in each bin are calculated and used to normalize the residuals; the mean is removed and the residuals are divided by their standard deviation in each bin. In this step, an additional margin for the sample means and standard deviations, i.e., μ_{AGDV} and σ_{AGDV}, is considered because the amount of data may be insufficient to ensure the stringent integrity requirement of 10^{-7} for ARAIM applications. The upper bound of the sample standard deviation can be derived by considering

a χ^2-distributed-based confidence interval with a $1-\alpha$ confidence level. In this work, a 95% confidence level was considered, and the length of the confidence level is determined as follows (Hayter, 2012):

$$\hat{\sigma}_{AGDV} = \sqrt{\frac{(n-1)}{\chi^2_{\frac{\alpha}{2},n-1}}}\,\sigma_{AGDV} \tag{16}$$

where n is the number of samples in each bin and σ_{AGDV} is the standard deviation of the sample distribution in each bin. The corresponding two-sided confidence interval for the sample mean is then constructed as follows:

$$\left[\mu_{AGDV} - \left(\frac{t_{\frac{\alpha}{2},n-1}}{\sqrt{n}}\right)\sigma_{AGDV},\ \mu_{AGDV} + \left(\frac{t_{\frac{\alpha}{2},n-1}}{\sqrt{n}}\right)\sigma_{AGDV}\right] \tag{17}$$

where $t_{\frac{\alpha}{2},n-1}$ represents the critical point of the t-distribution with $n-1$ degrees of freedom for which the t-distributed random variable takes the tail probability of $\alpha/2$.

In this investigation, the upper bound of the interval is taken as the worst bound of the sample mean $(\hat{\mu}_{AGDV})$ for each bin:

$$\hat{\mu}_{AGDV} = \mu_{AGDV} + \left(\frac{t_{\frac{\alpha}{2},n-1}}{\sqrt{n}}\right)\sigma_{AGDV} \tag{18}$$

Based on the distribution of normalized AGDV residuals, the inflation factor (L) is then determined in each bin, as shown in the previous position domain analysis. Lastly, the "σ_{AGDV} overbound" for each bin (see Figure 6 (right)) is computed as follows:

$$\sigma_{AGDV,\,overbound} = \left|\hat{\mu}_{AGDV}\right| + L\hat{\sigma}_{AGDV} \tag{19}$$

Figure 6 (right) shows the overbound result, i.e., $\sigma_{AGDV,\,overbound}$. The estimated overbounds (magenta curve with asterisks) are similar to the one-sigma values (red curve with circles) at elevation angles lower than 45°. In contrast, the estimated overbounds reach approximately 0.4 m at elevation angles higher than 45°, while the one-sigma values are below approximately 0.15 m. Table 6 shows the overbounding sigma values for each bin.

In this section, the AGDV-induced error has been considered within a random sigma value as a function of elevation angle. In the next section, the error effect is considered as the worst-case bias in the PL calculation.

4.3 | Modeling the User Antenna Effect as the Worst-Case Bias Term

This section considers the AGDV error effect with respect to the VPL in the worst-case scenario by adding a new user antenna bias bound to PLs derived by the baseline user algorithm (see Equation (10)) as follows:

$$VPL = VPL_{user} + \sum_i^n \left|\boldsymbol{S_i}\right| b_{AGDV,i} \tag{20}$$

TABLE 6
AGDV Error as a Function of Elevation Angle

Elevation (deg)	$\sigma_{AGDV,overbound}$ (m)
5 <	0.3719
10 <	0.3435
15 <	0.3278
20 <	0.3123
25 <	0.2911
30 <	0.2595
35 <	0.2154
40 <	0.1584
45 <	0.1393
50 <	0.1747
55 <	0.2291
60 <	0.2935
65 <	0.3544
70 <	0.4027
75 <	0.4324
80 <	0.4373
85 <	0.4232

Here, VPL_{user} denotes the VPL computed by the baseline user algorithm. S_i indicates each measurement error projection into the vertical position domain, and $b_{AGDV,i}$ represents the antenna bias error for each pseudorange measurement. In this study, two types of observables were used: AGDV errors derived from the DUFMAN work (Circiu et al., 2019) and an upper bound outlined by the antenna MOPS (RTCA SC-159, 2018). Because Circiu et al. (2021) demonstrated that the MOPS limit stated in DO-373 can overbound the observed AGDV for the L1/E1 and L5/E5a bands, this paper applies the limit in DO-373 for simulation purposes.

5 | SIMULATION RESULTS

In this section, we conduct V-ARAIM service volume simulations for LPV-200. All simulations are performed via the Stanford MAAST for ARAIM (*MATLAB Algorithm Availability Simulation Tool*, 2021) with some modifications and the key simulation parameters listed in Table 2. The following six simulation scenarios are examined, as summarized in Table 7.

Case 1: The legacy user CNMP measurement error model (Blanch et al., 2015) is used.

Case 2: The DUFMAN multipath and AGDV error models are applied (Circiu et al., 2021).

Case 3: The DUFMAN multipath model is used, and the overbounding sigma values in the range domain, i.e., σ_{AGDV} in Equation (19), are used for the AGDV error contribution.

Case 4: The DUFMAN multipath model is used, and the overbounding sigma values derived in the position domain, i.e., σ_{AGDV} in Table 4 and Table 5, are used for the PL equation in Equation (11).

Case 5: The DUFMAN multipath model is applied, and the AGDV error bound based on the actual antenna error measurements is added to the VPL (see Equation (20)).

TABLE 7
Simulation Scenarios

Scenario	Multipath	AGDV error	Receiver noise
Case 1		Baseline CNMP (Blanch et al., 2015)	0.04 m
Case 2		$\sigma_{MP\&ADGV,DUFMAN}$ (RMS)	
Case 3	$\sigma_{MP,DUFMAN}$	σ_{AGDV} for different elevation angles	
Case 4	$\sigma_{MP,DUFMAN}$	$\sigma_{SS,AGDV}$, σ_{AGDV}, and b_{AGDV} for different fault hypotheses	
Case 5	$\sigma_{MP,DUFMAN}$	$\lvert S\rvert b_{AGDV}$ (actual bias measurements (Caizzone, Circiu, Elmarissi, Enneking, & Winterstein, 2019))	
Case 6	$\sigma_{MP,DUFMAN}$	$\lvert S\rvert b_{AGDV}$ (MOPS upper bound (RTCA SC-159, 2018))	

Case 6: The DUFMAN multipath model is applied, and the AGDV error bound based on the MOPS upper bound (RTCA SC-159, 2018) is added to the VPL.

Global ARAIM VPL maps for the cases listed above are also compared with the result from the baseline scenario in which the AGDV errors are lumped together with the legacy GPL L1 MOPS multipath model (RTCA SC-159, 2004).

5.1 | Impact of the New Combined Multipath and AGDV Model (Case 1 vs. Case 2)

We first assess the baseline performance based on the legacy CNMP model. Figure 7 (left) shows the 99.5% LPV-200 availability map as a function of user location when the legacy model is applied as described for Case 1. The availability indicates the percentage of time during which the user horizontal/vertical PL (H/VPL) is less than the corresponding horizontal/vertical alert limit (H/VAL). In the availability map, the coverage for users with availability higher than 99.5% corresponds to approximately 90.54% of the map. This coverage indicates the fraction of users within the region that had a time availability of 99.5% or greater, represented as purple or dark purple regions. Next, we examine the DUFMAN multipath and antenna model, as described for Case 2, by replacing the legacy multipath model (i.e., σ_{MP} in Equation (1)) with the modified $\sigma_{MP\&AGDV}$. Because the receiver noise contribution was not considered in the construction of the DUFMAN multipath model (Circiu et al., 2021), the existing receiver code noise model is still included, as shown below:

$$\sigma_{CNMP} = \sqrt{\sigma^2_{MP\&AGDV,DUFMAN} + \left(\frac{f^4_{L1} + f^4_{L5}}{\left(f^2_{L1} - f^2_{L5}\right)^2}\right)\sigma^2_{Noise}} \tag{21}$$

Figure 7 (right) shows the availability map obtained when the newly derived multipath and user antenna error models are used. This figure shows that the global availability increases by approximately 5% if the new DUFMAN multipath and user antenna error models are applied for the ARAIM fault detection and PL computation. This result occurs because, as discussed earlier, the modified multipath model for GPS L1/L5 and Galileo E1/E5a has lower bounds than the legacy GPS L1 multipath model, particularly for low satellite elevation angles.

Figure 8 shows 99.5% VPL maps for the two cases, and Figures 9 and 10 present other requirements for LPV-200, i.e., σ_{acc} and the effective monitor threshold (EMT), which are criteria that determine the availability performance. In this

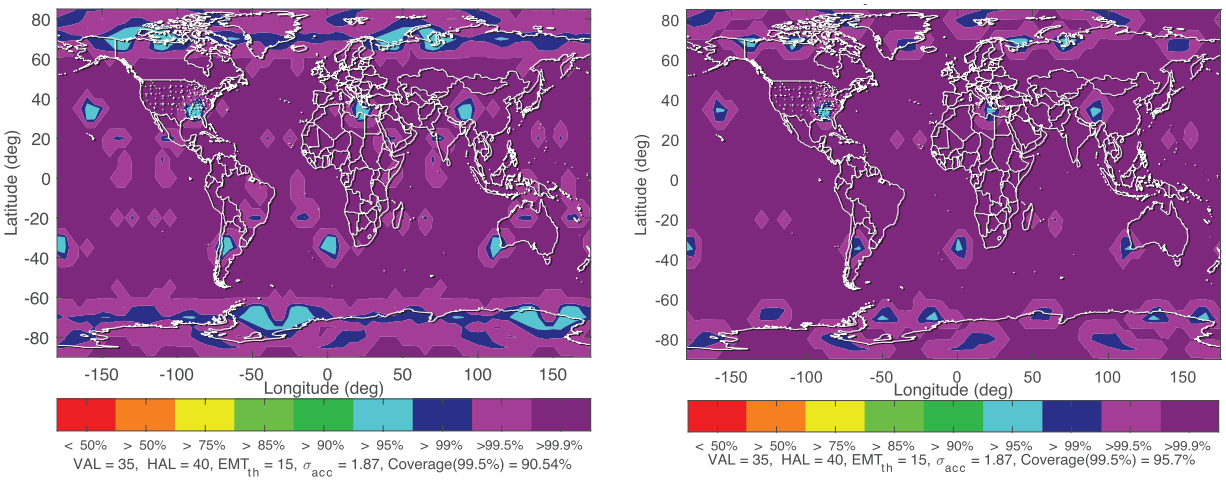

FIGURE 7 99.5% availability map for LPV-200 when the legacy noise and multipath model are applied (left) and a corresponding availability map for when the newly derived multipath and user antenna model (i.e., DUFMAN $\sigma_{MP\&ADGV}$ in Equation (2)) are used for the ARAIM fault detection algorithm (right)
The simulation parameters listed in Table 2, including ISM parameters, were applied.

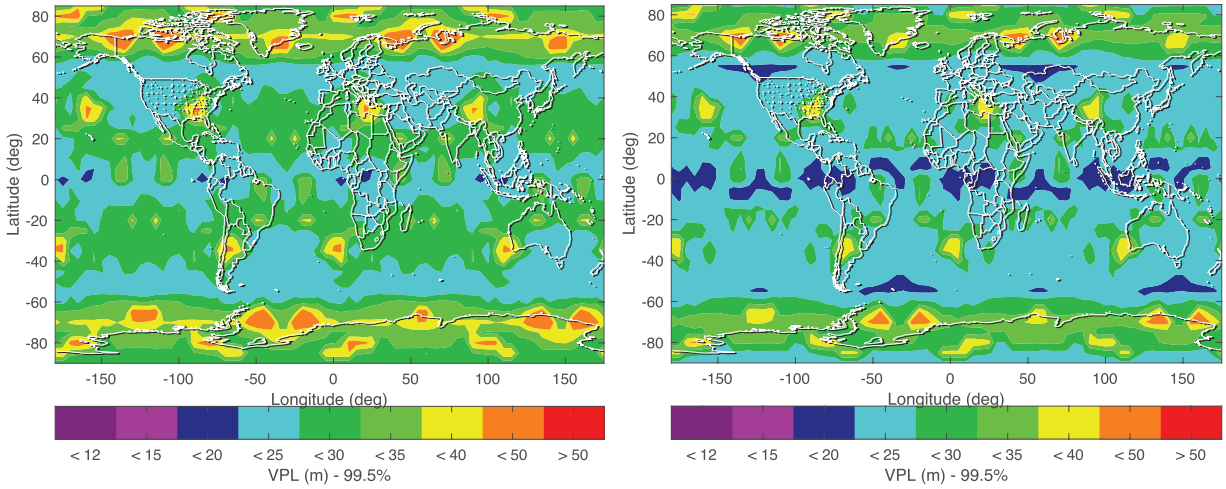

FIGURE 8 99.5% VPL map based on the legacy noise and multipath mode (left) and DUFMAN $\sigma_{MP\&ADGV}$ (right)

study, the thresholds for σ_{acc} and EMT are 1.87 m and 15 m for 99.5% LPV-200, respectively (Working Group C. ARAIM Technical Subgroup, 2016). σ_{acc} indicates the standard deviation of the vertical position solution used for the accuracy requirement. The EMT is defined as the maximum value of detection thresholds of faults whose prior probability is equal to or higher than a given requirement (Blanch et al., 2015). As shown in Figure 8, the VPL magnitude decreases in the majority of regions in the map when the new model is applied. However, because the alert limit for LPV-200 operation is 35 m (Working Group C. ARAIM Technical Subgroup, 2016), a comparison of Figures 7 and 8 shows that effective improvements with respect to availability can be achieved in high-latitude regions while VPL reductions in mid-latitude and equatorial regions are not actually counted. Thus, despite the noticeable decrease in VPL in almost all regions, an improvement of 5% can be achieved with respect to availability.

It is evident from Figure 9 and Figure 10 that σ_{acc} and EMT improve in the majority of areas if the less-conservative model is applied. In particular, the coverage in

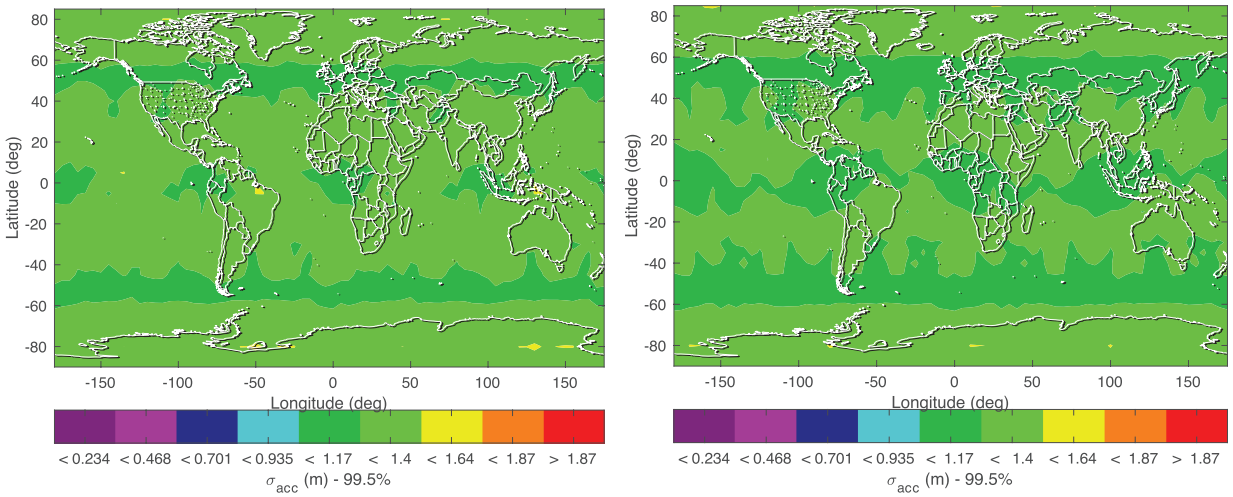

FIGURE 9 Standard deviation of the vertical position solution (σ_{acc}) based on the existing noise and multipath model (left) and based on DUFMAN $\sigma_{MP\&ADGV}$ (right)

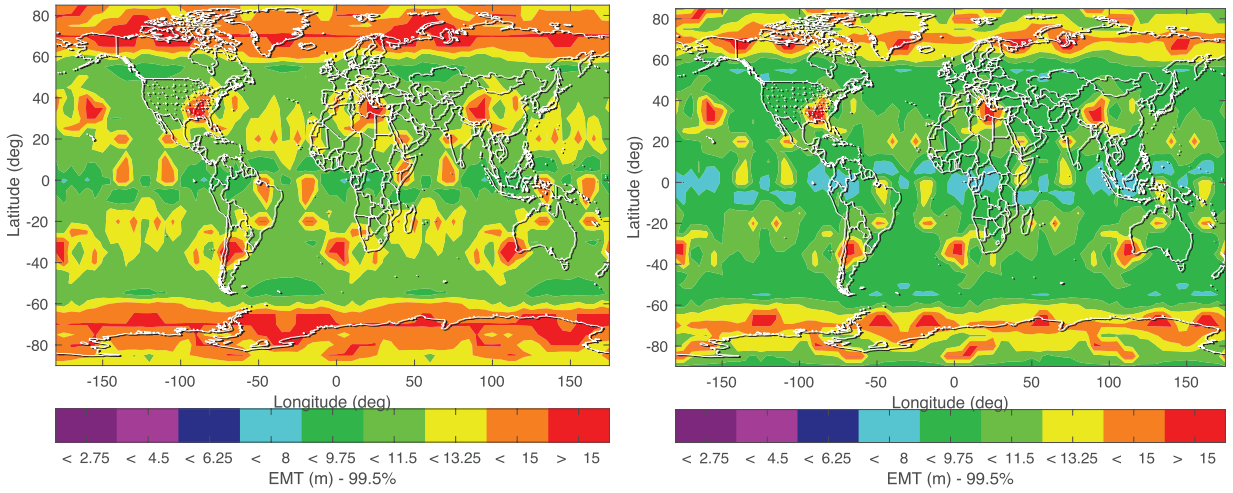

FIGURE 10 EMT based on the legacy noise and multipath model (left) and DUFMAN $\sigma_{MP\&ADGV}$ (right)`

which the EMT requirement, i.e., lower than 15 m, is met extends noticeably in high-latitude areas, resulting in an availability coverage improvement. In contrast, the σ_{acc} requirement is already met for both cases.

However, because the combined error model ($\sigma_{MP\&AGDV}$) was considered, the improvements shown above may be due to the combined effect of multipath and AGDV contributions. Evaluating the extent of improvement that can be achieved by the new AGDV error model alone (or multipath model alone) is challenging because, unlike the new DUFMAN model in which the multipath and AGDV contributions are characterized separately, the contributions are mixed within the legacy model. Alternatively, to examine the AGDV impact in VPL, Figure 11 shows the difference between the VPL based on the combined model $\left(VPL_{\sigma_{MP\&AGDV}}\right)$ and that based on σ_{MP} $\left(VPL_{\sigma_{MP}}\right)$, i.e., with σ_{AGDV} removed from $\sigma_{MP\&AGDV}$ in Equation (2). It is shown that an additional increase of more than 1.3 m in the 99.5% VPL can result from σ_{AGDV} in high-latitude areas, where the availability coverage predominantly expands.

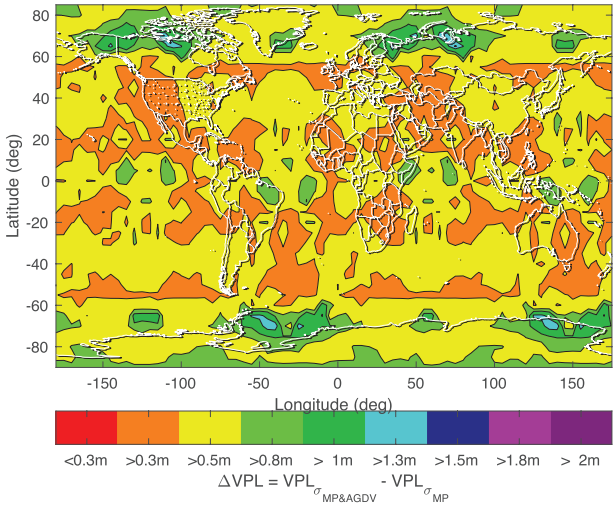

FIGURE 11 Difference between 99.5% VPL based on the combined $\sigma_{MP\&AGDV}\left(VPL_{\sigma_{MP\&AGDV}}\right)$ and that based on σ_{MP} instead of $\sigma_{MP\&AGDV}\left(VPL_{\sigma_{MP}}\right)$

However, this work is more focused on the AGDV error contribution, and such increases in VPL due to the AGDV error might be still optimistic because the DUFMAN model is an RMS-based model. Thus, as mentioned above, we further examine the impact of the AGDV error contribution in the worst-case scenario by taking different approaches to modeling the AGDV error in the following sections.

5.2 | Impact of AGDV-Induced Error Contribution for Different Modeling Approaches (Case 3 – Case 6)

Now that we have examined the impact of the new combined model ($\sigma_{MP\&AGDV}$) with respect to the legacy GPS CNMP model in the previous section, this section describes how the AGDV error affects the ARAIM performance when different modeling approaches are applied (see Cases 3–6 in Table 7) and evaluates the worst impact of the error.

As discussed earlier, in prior work (Circiu et al., 2021), the Gaussian term $\sigma_{MP\&AGDV}$ in Equation (2) was derived in the form of an RMS. Because this investigation is focused on the AGDV error contribution, in this case, the new overbounding sigma term for the AGDV derived in the range domain is applied for the term $\sigma_{MP\&AGDV}$ while the same RMS multipath model is used. Figure 12 shows global maps in which the increase in the 99.5% VPL (left) and 99.5% HPL (right) is represented when the overbounding σ_{AGDV}, instead of the RMS bound, is applied for σ_{CNMP} in Equation (20). The results show that the maximum increase is approximately 0.7 m in the VPL and 0.3 m in the HPL, which is not significant enough to affect the global availability coverage.

Because the change in the PLs seems to be marginal for almost all regions in the map, we sought to investigate the impact of different error modeling methods on the VPL magnitude in greater detail. Thus, the VPLs computed in the availability simulation at a specific user location (110°W, 65°N) for a single day are shown in Figure 13. The VPL is calculated at this location because the 99.5% LPV-200 availability decreases/increases significantly in this region when the different error models are applied, as shown in Figure 7.

In Figure 13, the results for three scenarios are shown: Case 2, Case 3, and Case 4 from Table 7. Because the DUFMAN error model considers the RMS of the

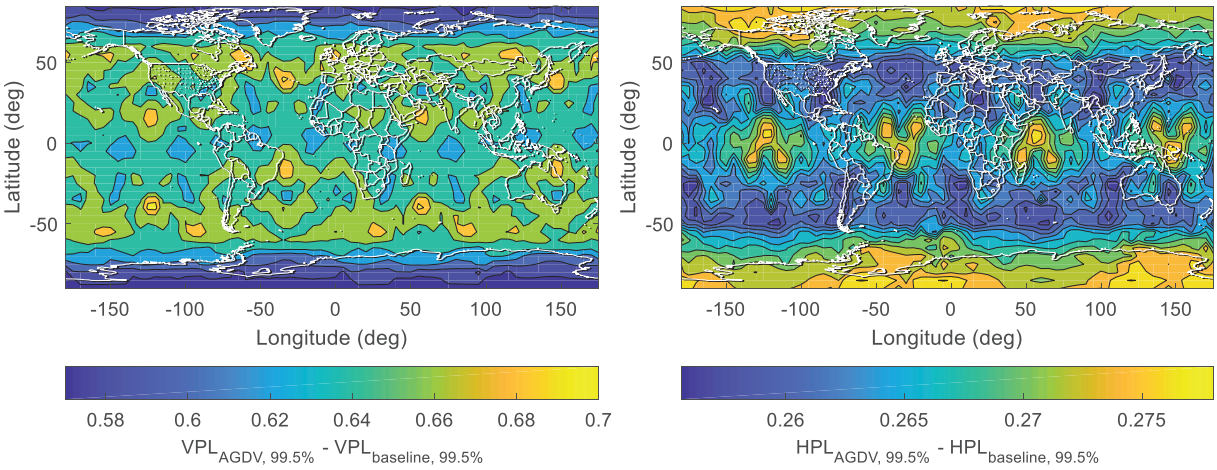

FIGURE 12 Increase in the VPL (left) and HPL (right) magnitude for Case 3
The maximum increase in the VPL and HPL is approximately 0.7 m and 0.3 m, respectively, when the AGDV effect (σ_{AGDV}) is considered for the PL calculation.

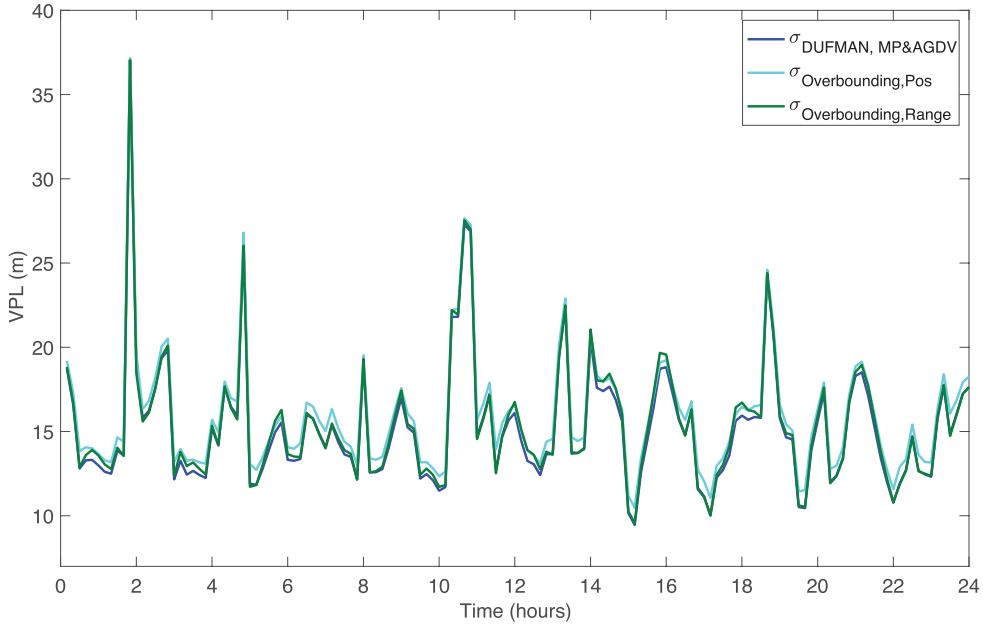

FIGURE 13 VPLs based on different error models: the DUFMAN model (Case 2 in Table 7) (blue), overbounding in the range domain (Case 3) (green), and overbounding in the position domain (Case 4) (light blue)

multipath and AGDV errors (i.e., Case 2), it results in an optimistic VPL (solid blue line). We also investigate the extent of VPL margin that can be achieved by applying different approaches to the user antenna error modeling. For this, the VPLs based on the overbounding sigma values in the range domain (Case 3) and position domain (Case 4) are plotted in Figure 13. The green curve and light blue curve represent the VPL for Cases 3 and 4, respectively. As expected, the AGDV error bound in the range domain results in a higher VPL than the RMS model-based VPL. In addition, for the most part, the VPLs based on the position domain overbounds are slightly higher than those based on the range domain overbounds. This result primarily arises from the fact that in the position domain approach, each sigma overbound for each fault mode was determined from the worst satellite geometry for each fault mode.

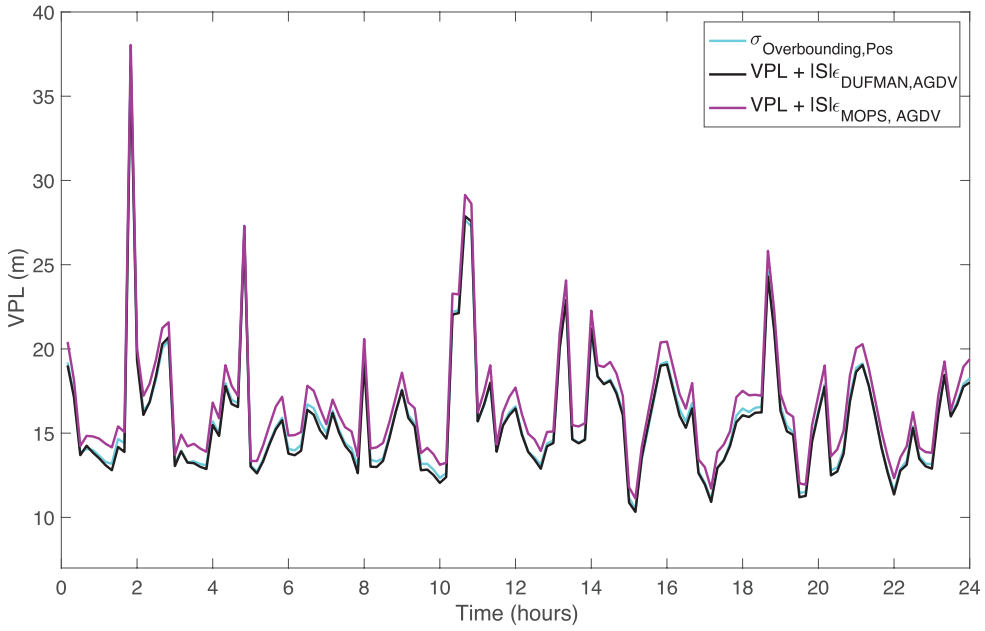

FIGURE 14 Comparison of VPLs for Case 4 (light blue), Case 5 (black), and Case 6 (magenta)

In Figure 14, the black line shows the VPL when the additional position bias term was applied for the VPL computation using DUFMAN AGDV error estimates. The VPL based on the bias term is comparable to that based on the position domain overbound (light blue). Lastly, the magenta line shows the VPL when the MOPS bounds on AGDV errors were applied for the VPL calculation as the additional bias term. As expected, considering the upper bounds within the bias term results in the worst impact on the VPL. Because the antenna chosen for this investigation had the worst performance among the antennas examined in DUFMAN and the corresponding AGDV errors were at the limit of the bound defined in the MOPS, the VPL results of the actual observables are not substantially different from those of the MOPS bounds.

The VPLs based on the six different cases are shown together in Figure 15. The results show that different improvements in the VPL can be achieved depending on the manner in which the AGDV effect is modeled and implemented at the algorithm level. As indicated in Figure 14, consideration of the MOPS bound within the bias term in the PL computation results in the worst impact on the VPL. To evaluate the impact of AGDV error in the worst-case scenario, Case 6 must be examined in greater detail. Figure 16 shows the difference between the VPL obtained from the MOPS bound $\left(VPL_{\sigma_{MP}\&MOPS}\right)$, which corresponds to the magenta line in Figure 15, and that based on the combined model $\left(VPL_{\sigma_{MP\&AGDV}}\right)$, where the AGDV error contribution is modeled as the RMS bound. An additional increase in VPL of more than 1.3 m, compared with the RMS model $\left(\text{i.e.}, VPL_{\sigma_{MP\&AGDV}}\right)$, is observed when the worst impact of the AGDV error is taken into account, and the additional margin results in an availability loss of approximately 1%. Note that the DUFMAN multipath model is applied to both $VPL_{\sigma_{MP}\&MOPS}$ and $VPL_{\sigma_{MP\&AGDV}}$.

However, considering that the VAL for LPV-200 is 35 m (see Figure 15), the impact of AGDV error on the LPV-200 ARAIM availability performance appears to not be of major relevance if we employ the newly proposed (or less-conservative) multipath and noise models.

The impact of the different AGDV models, including the combined DUFMAN model, on V-ARAIM has been presented under various scenarios. However,

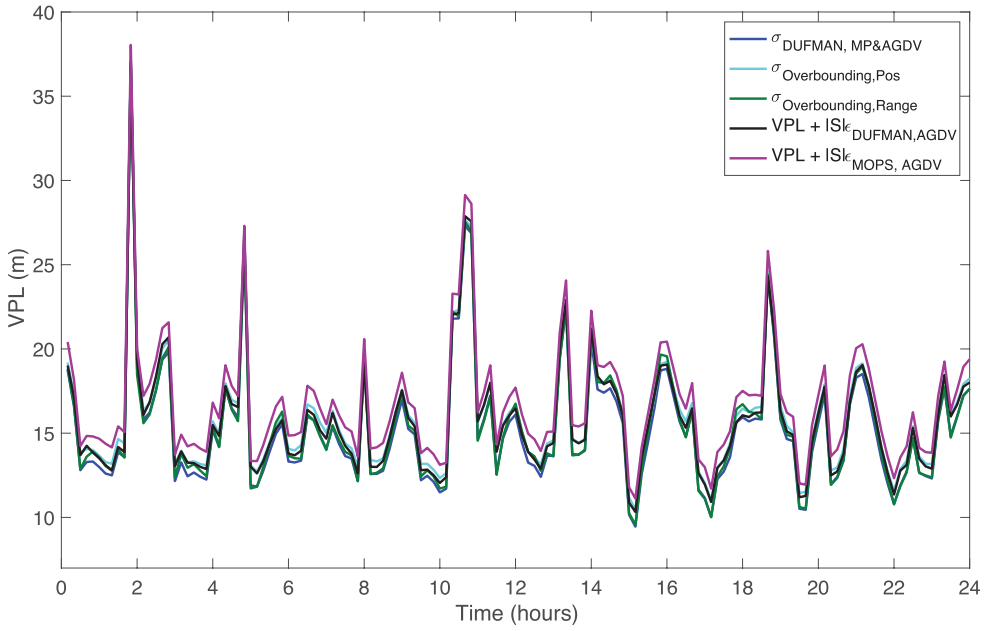

FIGURE 15 VPLs for the different scenarios from Cases 2–6

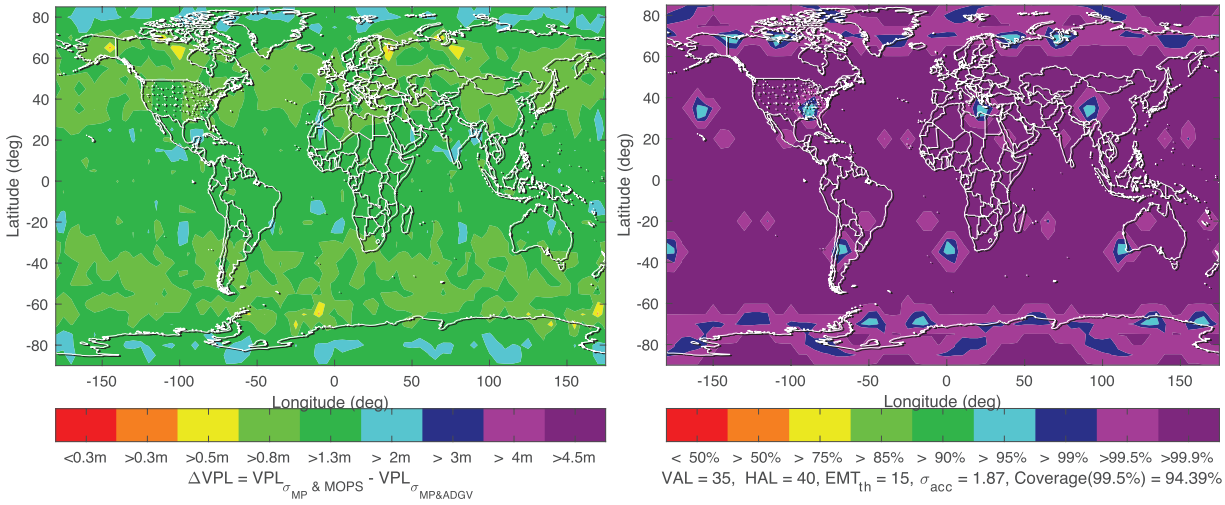

FIGURE 16 Difference between 99.5% VPLs obtained by considering the MOPS bound on AGDV error within the PL computation $\left(VPL_{\sigma_{MP}\&MOPS}\right)$ and the VPL based on the combined multipath and AGDV model $\left(VPL_{MP\&AGDV}\right)$ (left); 99.5% availability for LPV-200 when the worst PL $\left(VPL_{\sigma_{MP}\&MOPS}\right)$ is applied (right)

considering that ARAIM should begin with horizontal service only, i.e., horizontal ARAIM (H-ARAIM), we also examine how the different models affect the HPL. For the initial implementation of H-ARAIM, the ISM parameters in Table 2 have been considered for GPS and Galileo by the community (Working Group C. ARAIM Technical Subgroup, 2016), and we applied the same parameters. Figure 17 shows HPLs for the different AGDV modeling approaches, similar to Figure 15. Only the worst-case bias scenario (Case 6) results in an HPL increase of 1–1.5 m. In contrast, the other methods result in comparable HPLs, which is in line with the VPL comparison in Figure 15. Because an HAL of 185 m is defined for required navigation performance (RNP) 0.1, which is the target

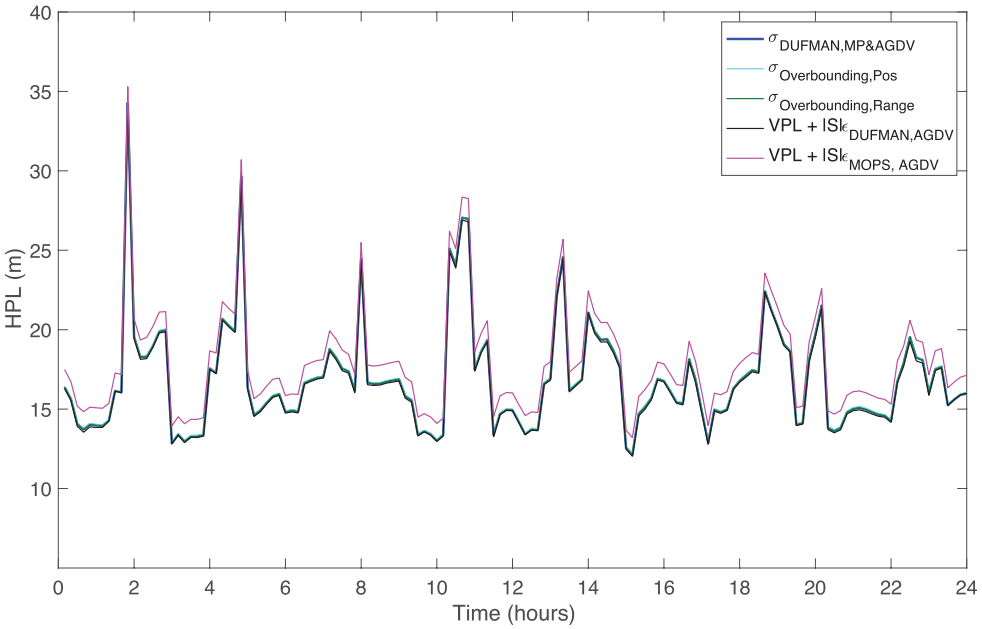

FIGURE 17 HPLs for the different scenarios from Cases 2–6

performance of H-ARAIM, it is evident that an improvement in availability will not be observed. Thus, only the HPLs are compared in this section.

In this section, we investigated the effect of AGDV on ARAIM performance in different aspects, including the protection bounds, position accuracy, and EMT, by applying a baseline user algorithm and different multipath and AGDV models. It should be noted, however, that this analysis is based on limited results (e.g., the AGDV error model for a specific antenna type), and variations in parameters such as the user range accuracy value employed in the simulations could lead to different results.

6 | CONCLUSION

In this paper, we have applied several approaches to model the user antenna bias error within a bias term and as a random process sigma term in both the position and range domains and assessed the ARAIM performance for the different error modeling approaches. The results showed a maximum increase of approximately 5% in the 99.5% global availability for LPV-200 when the newly constructed DUFMAN multipath and antenna error models for GPS L1/L5 and Galileo E1/E5a were accounted for in the ARAIM fault detection algorithm. A preliminary assessment also showed that the worst impact of the AGDV error contribution resulted in an availability loss of only about 1% for LPV-200 with the current standard, i.e., $\sigma_{URA} = 1\,m$, for both GPS and Galileo.

These findings extend those of a recent investigation by Griggs et al. (2020), confirming that even if the worst-case user antenna error contribution, i.e., the dual-frequency dual-constellation MOPS bound, is integrated within the nominal bias term of the ARAIM user algorithm, the user antenna impact on the 99.5% LPV-200 availabliity would be marginal. Most notably, to our knowledge, this is the first study to rigorously examine the effect of user antenna bias errors on ARAIM performance by isolating this contribution as a deterministic and stochastic error.

However, some limitations are worth noting. Although extensive simulations supported our findings with different realistic modeling scenarios, the results presented in this study were derived from a limited set of ISM parameters such as σ_{URA}, the constant fault probability of a GPS constellation-wide fault, and a baseline fault detection algorithm. The influence of AGDV error on ARAIM performance may differ depending on the underlying assumptions of parameters and algorithms. Thus, future work should include follow-up work designed to reassess the impact across a wide range of the ISM parameters with an optimized estimation algorithm (Blanch et al., 2015).

ACKNOWLEDGMENTS

This research has been partially funded by EU project DARP.

REFERENCES

Blanch, J., Walter, T., & Enge, P. (2019). Gaussian bounds of sample distributions for integrity analysis. *IEEE Transactions on Aerospace and Electronic Systems*, *55*(4), 1806–1815. https://doi.org/10.1109/TAES.2018.2876583

Blanch, J., Walter, T., Enge, P., Lee, Y., Pervan, B., Rippl, M., Spletter, A., & Kropp, V. (2015). Baseline advanced RAIM user algorithm and possible improvements. *IEEE Transactions on Aerospace and Electronic Systems*, *51*(1), 713–732. https://doi.org/10.1109/TAES.2014.130739

Caizzone, S., Circiu, M.-S., Elmarissi, W., Enneking, C., & Felux, M. (2019). Antenna influence on global navigation satellite system pseudorange performance for future aeronautics multifrequency standardization. *NAVIGATION*, *66*(1), 99–116. https://doi.org/10.1002/navi.281

Caizzone, S., Circiu, M.-S., Elmarissi, W., Enneking, C., & Winterstein, A. (2019). Airborne antenna and multipath error characterization for DFMC error standardization. *Proc. of the 32nd International Technical Meeting of the Satellite Division of the Institute of Navigation (ION GNSS+ 2019),* Miami, FL, 1453–1463. https://doi.org/10.33012/2019.16908

Circiu, M., Caizzone, S., Felux, M., Enneking, C., Rippl, M., & Meurer, M. (2020). Development of the dual-frequency dual-constellation airborne multipath models. *NAVIGATION*, *67*(1), 61–81. https://doi.org/10.1002/navi.344

Circiu, M.-S., Caizzone, S., Enneking, C., Fohlmeister, F., Rippl, M., Meurer, M., Felux, M., Gulie, I., Rüegg, D., Griggs, J., Lazzerini, R., Hagemann, F., Tranchet, F., Bouniol, P., & Sgammini, M. (2021). Final results on airborne multipath models for dual-constellation dual-frequency aviation applications. *Proc. of the 2021 International Technical Meeting of the Institute of Navigation,* 714–727. https://doi.org/10.33012/2021.17862

Circiu, M.-S., Felux, M., Caizzone, S., Enneking, C., Fohlmeister, F., Rippl, M., Gulie, I., Rueegg, D., Griggs, J., Lazzerini, R., Hagemann, F., Tranchet, F., Bouniol, P., & Sgammini, M. (2019). Initial results for dual constellation dual-frequency multipath models. *Proc. of the 32nd International Technical Meeting of the Satellite Division of the Institute of Navigation (ION GNSS+ 2019),* Miami, FL, 1401–1417. https://doi.org/10.33012/2019.16906

Circiu, M.-S., Felux, M., Caizzone, S., Enneking, C., Fohlmeister, F., Rippl, M., Sgammini, M., & Chatre, E. (2020). Airborne multipath and antenna error models from the DUFMAN project. *Proc. of the ICAO Navigation System Panel Meeting, Montreal*.

DeCleene, B. (2000). Defining pseudorange integrity – Overbounding. *Proc. of the 13th International Technical Meeting of the Satellite Division of the Institute of Navigation (ION GPS 2000),* Salt Lake City, UT, 1916–1924. https://www.ion.org/publications/abstract.cfm?articleID=1603

EUROCAE. (2019). *ED-259-Minimum operational performance standards for Galileo—Global positioning system—Satellite-based augmentation system airborne equipment*.

Griggs, J., Rippl, M., Caizzone, S., & Circiu, M.-S. (2020). Effects of preliminary DFMC multipath models on ARAIM performance. *Proc. of the 2020 International Technical Meeting of the Institute of Navigation,* San Diego, CA, 174–188. https://doi.org/10.33012/2020.17136

Haines, B., Bertiger, W., Desai, S., Harvey, N., Sibois, A., & Weiss, J. (2012). Characterizing the GPS satellite antenna phase- and group-delay variations: Latest results. *Proc. of the 2012 IGS Workshop*. https://files.igs.org/pub/resource/pubs/workshop/2012/Poland%202012%20-%20P08%20Haines%20PO31.pdf

Harris, M., Schlais, P., Murphy, T., Joseph, A., Kazmierczak, J., & Aerospace, C. (2020). GPS and GALILEO airframe multipath error bounding method and test results. *Proc. of the 33rd International Technical Meeting of the Satellite Division of the Institute of Navigation (ION GNSS+ 2020),* St. Louis, MO, 114–139. https://doi.org/10.33012/2020.17568

Hayter, A. J. (2012). *Probability and statistics for engineers and scientists* (4th ed). Brooks/Cole, Cengage Learning.
IS-GPS-200N. (2022). *NAVSTAR GPS space segment/navigation user segment interfaces*.
Kaplan, E. D., & Hegarty, C. (2017). *Understanding GPS/GNSS: Principles and applications* (3rd ed.). Artech House.
Lee, J., Pullen, S., Datta-Barua, S., & Enge, P. (2007). Assessment of ionosphere spatial decorrelation for global positioning system-based aircraft landing systems. *Journal of Aircraft*, *44*(5), 1662–1669. https://doi.org/10.2514/1.28199
MATLAB algorithm availability simulation tool. (2021). https://gps.stanford.edu/resources/software-tools/maast
Murphy, T., Brenner, M., Cas-Spo, H., & Pullen, D. S. (2000). Development of the LAAS accuracy models. *Proc. of the 13th International Technical Meeting of the Satellite Division of the Institute of Navigation (ION GPS 2000),* Salt Lake City, UT, 1212–1223. https://www.ion.org/publications/abstract.cfm?articleID=1523
Murphy, T., Snow, R., & Braasch, M. (1996). GPS multipath on large commercial air transport airframes. *NAVIGATION*, *43*(4), 397–406. https://doi.org/10.1002/j.2161-4296.1996.tb01928.x
OS SIS ICD. (2021). *Galileo OS signal-in-space interface control document*.
Perea, S., Meurer, M., Rippl, M., Belabbas, B., & Joerger, M. (2017). URA/SISA analysis for GPS and Galileo to support ARAIM. *NAVIGATION*, *64*(2), 237–254. https://doi.org/10.1002/navi.199
Rife, J., Pullen, S., Enge, P., & Pervan, B. (2006). Paired overbounding for nonideal LAAS and WAAS error distributions. *IEEE Transactions on Aerospace and Electronic Systems*, *42*(4), 1386–1395. https://doi.org/10.1109/TAES.2006.314579
RTCA. (2006). *DO 301—Minimum operational performance standards for global navigation satellite system (GNSS) airborne active antenna equipment for the L1 frequency band*.
RTCA SC-159. (2004). *DO 245A - Minimum aviation system performance standards for the LAAS*. RTCA document DO-245A.
RTCA SC-159. (2016). *DO 229E - Minimum operational performance standards (MOPS) for global positioning system/satellite-based augmentation system airborne equipment*.
RTCA SC-159. (2018). *DO 373—MOPS for GNSS airborne active antenna equipment for the L1/E1 and L5/E5a frequency bands*.
Walter, T., & Blanch, J. (2015). KEYNOTE - Characterization of GNSS clock and ephemeris errors to support ARAIM. *Proc. of the ION 2015 Pacific PNT Meeting,* Honolulu, HI, 920–931. https://www.ion.org/publications/abstract.cfm?articleID=12769
Walter, T., Gunning, K., Eric Phelts, R., & Blanch, J. (2018). Validation of the unfaulted error bounds for ARAIM: Validation of the unfaulted error bounds for ARAIM. *NAVIGATION*, *65*(1), 117–133. https://doi.org/10.1002/navi.214
Wanninger, L., Sumaya, H., & Beer, S. (2017). Group delay variations of GPS transmitting and receiving antennas. *Journal of Geodesy*, *91*(9), 1099–1116. https://doi.org/10.1007/s00190-017-1012-3
Working Group C. ARAIM Technical Subgroup. (2016). *Milestone 3.0 report*. EU-US cooperation on satellite navigation.

How to cite this article: Bang, E., Circiu, M.-S., Caizzone, S., Rippl, M., Garcia Crespillo, O. (2024). Effect of user antenna group delay variation error on advanced RAIM. *NAVIGATION, 71*(1). https://doi.org/10.33012/navi.624

APPENDIX

This section provides more details of the user CNMP model used for the baseline ARAIM user algorithm. The CNMP model for L1/L5 is based on two different error sources: multipath and receiver tracking noise error. The multipath is modeled by Airframe Multipath Designator A for GPS L1 (Murphy et al., 2000):

$$\sigma_{MP,i} = 0.13 + 0.53 * e^{\left(-\frac{\theta_i}{10\,deg}\right)} \tag{A1}$$

TABLE A1
Galileo E1/E5a User Error Model According to Elevation Angle (Blanch et al., 2015)

Elevation (deg)	$\sigma_{CNMP,GAL}$ (m)
5°	0.4529
10°	0.3553
15°	0.3063
20°	0.2638
25°	0.2593
30°	0.2555
35°	0.2504
40°	0.2438
45°	0.2396
50°	0.2359
55°	0.2339
60°	0.2302
65°	0.2295
70°	0.2278
75°	0.2297
80°	0.2310
85°	0.2274
90°	0.2277

The noise contribution is modeled by AAD-A for GPS L1 code noise:

$$\sigma_{Noise,i} = 0.15 + 0.43 * e^{\left(-\frac{\theta_i}{6.9\,deg}\right)} \tag{A2}$$

A lookup table given as a function of elevation angle (see Table A1) has been used for Galileo E1/E5a for predicting the performance in the frame of ARAIM (Blanch et al., 2015).